Virtual element technique for computational homogenization problems

E. Artioli*, S. Marfia†, E. Sacco‡

Abstract

In this contribution, the virtual element method (VEM) is adopted for performing homogenization analyses of composites characterized by long fibre inclusions. The homogenization problem is briefly reviewed. Then, the procedure for constructing a virtual element is illustrated. In this context, a new virtual element is proposed for the micromechanical analysis of long fibre composites. It is a plane element, which is able to perform 3D analyses, characterized by three degree of freedoms per node that represent the displacement components in the three-dimensional space. Numerical examples are developed for assessing the ability of the VEM in efficiently solving the homogenization problem. Elements characterized by different number of edges are used in the numerical applications.

1 Introduction

Composite materials are used in several fields of engineering applications. The development of new and innovative composite materials together with the enhancement of material models and of computational tools promoted the implementation of effective numerical procedures for the accomplishment of sophisticated and accurate stress analyses of composite structural elements.

The issue of the multiscale analysis is very actual in structural mechanics. At the structural level the finite element method is generally adopted. At the material scale a representative volume element (RVE), containing all the pecularity of the composite material, is studied in order to recover the overall behavior of the composite. To this aim classical analytical homogenization procedures, such as Eshelby, self consistent and Mori Tanaka approach [14], could be adopted. These techniques have also been extended to take into account the nonlinear behavior of the constituents [9, 11]. On the other hand also numerical homogenization techniques can be adopted. In particular,

*Department of Civil Engineering and Computer Science, University of Rome Tor Vergata, Via del Politecnico 1, 00133 Rome, Italy, artioli@ing.uniroma2.it

†Department of Civil and Mechanical Engineering, University of Cassino and Southern Lazio, Via G. Di Biasio 43, 03043 Cassino, Italy, marfia@unicas.it

‡Department of Structures for Engineering and Architecture, University of Naples Federico II, Via Claudio 21, 80125 Naples, Italy, elio.sacco@unina.it

finite element micromechanical analyses could be developed to study the RVE and to determine the overall behavior of the composite. In particular, some micromechanical studies have been proposed in literature to study fibre reinforced composite adopting finite element analyses and taking into account the nonlinear behavior of the composite [8, 12, 13].

In the last years, the Virtual Element Method (VEM) has been proposed [1, 6]. It is a new and promising numerical method for solving partial differential equations; it can be viewed as an extension of Finite Element Methods to general polygonal and polyhedral elements. The VEM is characterized by strong mathematical foundations; it is quite simple in implementation and results efficient and accurate in several engineering problems and, in particular, in the linear elasticity problems [7, 2]. The VEM has also successfully been applied to solve structural problems characterized by material non-linearity such as plasticity, viscoelasticity and shape memory response [3].

In this paper, the VEM is adopted for performing homogenization analyses of composites characterized by long fibre inclusions. After formulating the homogenization problem, the VEM procedure is illustrated for the specific case of linear polynomial approximation of the displacement fields on the virtual element boundary. A new virtual element is developed for the 3D analyses of long fibre composites. In particular, it is a plane element with three degree of freedoms per node that are the displacement components in the three-dimensional space. Numerical examples are developed for assessing the ability of the VEM in efficiently solving the homogenization problem; validation being provided by comparison with an overkilling finite element solution.

2 Multiscale analysis of viscoplastic composites

The multiscale analysis of composite structures is based on the development of computations at two different scales, i.e. the scale of the structure (macro-scale) and the scale of the material (micro-scale). In particular, at the scale of the material a representative volume element (RVE) is introduced. If the two scales are very far, i.e. the characteristic length of the macro-scale is much greater than the scale of the RVE, the principle of the scale separation is invoked. In this case, it is assumed that the kinematics at macro and micro scale is uncoupled. According to the scale separation, the problem at the macro-scale is formulated without specifying the constitutive law, which is indeed determined by solving the micro-mechanical problem on the RVE and performing a homogenization procedure.

In this framework, let a global coordinate system be introduced at the macro-scale (X_1, X_2, X_3); the displacement field is defined by the vector $\mathbf{U} = \{U_1, U_2, U_3\}^T$ whose associated compatible strain is denoted by $\mathbf{E} = \{E_{11}, E_{22}, E_{33}, \Gamma_{12}, \Gamma_{23}, \Gamma_{13}\}^T$.

At the micro-scale, the special case of composite material characterized by a regular distribution of inclusions is considered. In particular, a periodic square array of long fiber composite is introduced; of course, other type of periodic arrangements can be

considered. In this case, a unit cell (UC) Ω with volume V can be introduced for deriving the overall response of the material. Let a local coordinate system be introduced at the micro-scale (x_1, x_2, x_3); a parallelepipedic unit cell with dimensions $2\,a_1 \times 2\,a_2 \times 2\,a_3$ parallel to the three coordinate axes x_1, x_2, x_3 is considered, as illustrated in figure 1. The x_3 axis is positioned to be parallel to the direction of the fiber axis. Note that a_3 can assume any positive value, as the material along the x_3-direction is homogeneous.

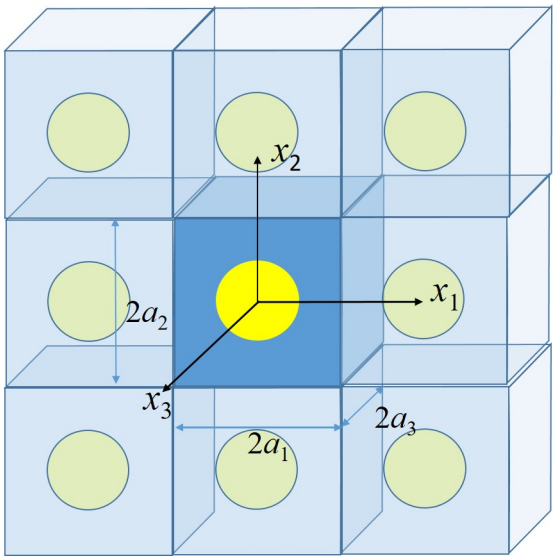

Figure 1: Schematic of a unit cell for a fiber-reinforced composite material with doubly periodic arrangement of fibers embedded into the matrix.

The strains evaluated at the macro-scale are considered as average strains occurring in the UC; thus, the displacement field at the micro-scale is represented in the form as:

$$\begin{aligned} u_1(x_1,x_2,x_3) &= E_{11}\,x_1 + \frac{1}{2}\Gamma_{12}\,x_2 + \frac{1}{2}\Gamma_{13}\,x_3 + u_1^\star(x_1,x_2,x_3) \\ u_2(x_1,x_2,x_3) &= \frac{1}{2}\Gamma_{12}\,x_1 + E_{22}\,x_2 + \frac{1}{2}\Gamma_{23}\,x_3 + u_2^\star(x_1,x_2,x_3) \\ u_3(x_1,x_2,x_3) &= \frac{1}{2}\Gamma_{13}\,x_1 + \frac{1}{2}\Gamma_{23}\,x_2 + E_{33}\,x_3 + u_3^\star(x_1,x_2,x_3)\,, \end{aligned} \tag{1}$$

where $\mathbf{u}^\star = \{u_1^\star,\, u_2^\star,\, u_3^\star\}^T$ is the perturbation displacement, resulting the periodic, due to the heterogeneity of the UC while $\mathbf{x} = \{x_1,\, x_2,\, x_3\}^T$ is the position vector of the typical point of Ω.

The perturbation displacement components $u_1^\star$, $u_2^\star$ and $u_3^\star$ have to satisfy the periodicity conditions along the three coordinate axes. In particular, the periodicity condition along the fiber direction together with homogeneity of the material along the same direction ensures that the periodic part of the displacements does not depend on x_3. Thus, it results $\mathbf{u}^\star = \mathbf{u}^\star\,(x_1, x_2)$ and the in-plane periodic conditions become:

$$\mathbf{u}^\star(x_1,x_2,a_3) = \mathbf{u}^\star(x_1,x_2,-a_3) \qquad \begin{matrix} x_1 \in [-a_1,a_1] \\ x_2 \in [-a_2,a_2] \end{matrix} \qquad \forall a_3\,. \tag{2}$$

From the formula (1), the strain at the typical point of Ω is:

$$\boldsymbol{\varepsilon}(x_1, x_2, x_3) \quad = \mathbf{E} + \boldsymbol{\varepsilon}^\star(x_1, x_2, x_3) \qquad \text{with } \boldsymbol{\varepsilon}^\star \quad = \mathbf{L}\mathbf{u}^\star \,, \tag{3}$$

where $\boldsymbol{\varepsilon}^\star$ represents the periodic part of the strain associated with the displacement $\mathbf{u}^\star$ and $\mathbf{L}$ the compatibility operator defined as:

$$\mathbf{L} = \begin{bmatrix} \cdot_{,1} & 0 & 0 \\ 0 & \cdot_{,2} & 0 \\ 0 & 0 & 0 \\ \cdot_{,2} & \cdot_{,1} & 0 \\ 0 & 0 & \cdot_{,2} \\ 0 & 0 & \cdot_{,1} \end{bmatrix} , \tag{4}$$

as all the derivatives with respect to x_3 are zero, because the displacement components do not depend on x_3.

Because of the periodicity conditions (2), the periodic strain $\boldsymbol{\varepsilon}^\star$ is characterized by null average on the UC.

The local stress field is evaluated accounting for the viscoplastic constitutive law illustrated in [Fritzen-Covezzi] as:

$$\boldsymbol{\sigma} \quad = \mathbf{C}\left(\boldsymbol{\varepsilon} - \boldsymbol{\pi}\right) , \tag{5}$$

where $\mathbf{C}$ is the elastic matrix that assumes different values in the fiber and in the matrix and $\boldsymbol{\pi}$ is the inelastic strain due to the viscoplastic effect.

The evolution of the viscoplastic strain $\boldsymbol{\pi}$ is assumed to be governed by a Mises yield domain in a framework of associate plasticity [**?**]. The yield function defining the elastic domain is given by

$$f\left(\boldsymbol{\sigma}, r\right) = q - \left(\sigma_y - r\right) \qquad \text{with} \quad q = \sqrt{\frac{3}{2}}\left\|\boldsymbol{\sigma}'\right\|_2 , \quad r = -H\alpha \,, \tag{6}$$

where q is the equivalent Mises stress, r is the isotropic hardening stress, σ_y is the yield stress, $\boldsymbol{\sigma}'$ is the second invariant of the deviatoric part of the stress, H is the hardening parameter and α is the accumulated plastic strain. The dissipation potential governing the inelastic strain evolution is introduced as:

$$\Phi^*(\boldsymbol{\sigma}, r) = \begin{cases} \sqrt{\frac{2}{3}}\frac{\dot{\varepsilon}_0 \sigma_D}{\epsilon+1}\left(\frac{f(\boldsymbol{\sigma},r)}{\sigma_D}\right)^{\epsilon+1} & f(\boldsymbol{\sigma}, r) > 0 \\ 0 & f(\boldsymbol{\sigma}, r) \leq 0 \end{cases} \tag{7}$$

with $\dot{\varepsilon}_0$ being a reference strain rate, $\epsilon \geq 1$ the dimensionless rate sensitivity parameter

and σ_D a (constant) drag stress. Then, the evolution laws are:

$$\dot{\alpha} = \frac{\partial \Phi^*(\boldsymbol{\sigma}, r)}{\partial r} = \sqrt{\frac{2}{3}}\dot{\varepsilon}_0 \left(\frac{f(\boldsymbol{\sigma}, r)}{\sigma_D} \right)^{\epsilon} \tag{8}$$

$$\dot{\boldsymbol{\pi}} = \frac{\partial \Phi^*(\boldsymbol{\sigma}, r)}{\partial \boldsymbol{\sigma}}, = \sqrt{\frac{2}{3}}\dot{\varepsilon}_0 \left(\frac{f(\boldsymbol{\sigma}, r)}{\sigma_D} \right)^{\epsilon} \frac{\partial f}{\partial \boldsymbol{\sigma}} = \dot{\alpha} \frac{\partial f}{\partial \boldsymbol{\sigma}}. \tag{9}$$

Note that $\dot{\alpha}$ in equation (9) can be interpreted as a nonnegative plastic multiplier [**?**].

Once the local stress is defined into the UC, the average stress is evaluated as:

$$\boldsymbol{\Sigma} = \frac{1}{V} \int_{\Omega} \boldsymbol{\sigma} \, dV \, . \tag{10}$$

3 Virtual element method

The virtual element (VE) formulation is presented in this section. First, a polygonal discretization of the unit cell Ω is performed, considering non overlapping polygons Ω_E characterized by a number of straight edges. The space of the approximated displacement field is defined element-wise by introducing local degrees of freedom, as in standard FE method, but differently from FE, the definition of the local displacement approximation is not fully explicit [7, 2]. Different accuracy can be introduced in the method, depending on the degree of the approximating functions for the displacement field.

Next, the fundamental steps describing a procedure for the development of a VE formulation for the problem described in the previous section, are given below.

1. Initially, the number m of straight edges defining the polygon Ω_E is set.

2. The displacements are approximated assuming an explicit representation on the boundary $\partial\Omega_E$ of each element Ω_E, while they are fully implicit in the interior of it. The approximated displacement, denoted in the following by $\mathbf{u}^{\star\, h}$, with h related to the mesh size, admits the following local FEM-like representation:

$$\mathbf{u}^{\star\, h} = \mathbf{N}_{\mathrm{b}} \, \tilde{\mathbf{U}}^{\star} + \mathbf{N}_{\mathrm{i}} \, \tilde{\mathbf{q}}^{\star} \, , \tag{11}$$

   where $\mathbf{N}_{\mathrm{b}}$ and $\mathbf{N}_{\mathrm{i}}$ are approximation functions arrays associated to boundary and interior degrees of freedom, respectively, whose properties will be specified in the following. Correspondingly, $\tilde{\mathbf{U}}^{\star}$ is the vector collecting the local degrees of freedom associated to nodes lying on the edges of $\partial\Omega_E$, while $\tilde{\mathbf{q}}^{\star}$ are interior degrees of freedom; the latter are not associated to any specific node, and are defined as suitable area-averaged moments of $\mathbf{u}^{\star\, h}$.

   Some comments on the above introduced virtual approximation functions and degrees of freedom are mandatory. First, $\tilde{u}_i^{\star\, h}$, the restriction of the displacement field to each edge e of the boundary polygonal line, is a polynomial of degree k;

i.e. it is set $\tilde{u}_i^{\star\,h} \in P_k(e)$. Note that for $k = 1$, a piecewise linear approximation function is adopted on $\partial\Omega_E$, so that two nodes are introduced on each edge; in other words, the vertices of the edges are the nodes of the boundary discretization. For $k = 2$, a piecewise quadratic approximation function is adopted on $\partial\Omega_E$, so that three nodes are introduced on each edge: the vertices plus the midpoint of each edge. In general, $(k-1)$ interior nodes will be selected upon each edge.

For any ~~a given order of accuracy~~ $k \geq 1$, the total number of local degrees of freedom for a polygon with m edges, then amounts to:

$$n = 3m + 3m(k-1) + 3\dim(P_{k-1}(\Omega_E)). \tag{12}$$

being $\dim(P_{k-1}(\Omega_E)) = k(k+1)/2$.

Representation (11) still retains the typical interpolatory character of the approximated field with respect to its degrees of freedom, in the sense explained in the following. As in standard FE technology, each $\tilde{\mathbf{U}}^\star$ degree of freedom represents the evaluation of the displacement field at the corresponding boundary node. Likewise, boundary shape functions will take unit value at the corresponding node and zero at the remaining ones. Differently, $\tilde{\mathbf{q}}^\star$ degrees of freedom are not attached to a specific spatial location, being area-averaged integral quantities specified previously.

3. In the spirit of a VEM micromechanical analysis of the unit cell nonlinear behavior, the equilibrium equation, written in the approximated variational form for the single VE, is expressed as:

$$0 = \int_{\Omega_E} [\boldsymbol{\varepsilon}(\delta\mathbf{u}^{\star\,h})]^T \, \boldsymbol{\sigma} \left(\boldsymbol{\varepsilon}(\mathbf{u}^{\star\,h}) + \mathbf{E}\right) dA \,. \tag{13}$$

4. As the approximated displacement field $\mathbf{u}^{\star\,h}$ is not explicit inside the element, but only on the boundary $\partial\Omega_E$, the gradient cannot be computed and, consequently, an explicit expression of strain is not available. Thus, a projector operator Π is introduced to approximate the strain associated to the displacement field. Such an operator is explicitly computable, and defined on the basis of the two fundamental requirements.

   - First requirement for Π:

$$\Pi(u_i^{\star\,h}) \in P_{k-1}^{6\times 1}\left(\Omega_E\right), \tag{14}$$

     that is a (6×1) vector-valued polynomial function of degree $k-1$ over Ω_E which, in general, can be represented as:

$$\boldsymbol{\varepsilon}^P = \mathbf{N}^P \, \hat{\boldsymbol{\varepsilon}} \tag{15}$$

where the matrix $\mathbf{N}^P$ is a $6 \times 6\dim(P_{k-1})$ matrix with identity blocks (indicated in the following with $\mathcal{I}_6$) premultiplied by the monomials of an ordered basis of P_{k-1} and the vector $\hat{\boldsymbol{\varepsilon}}$ contains the corresponding coefficients; in particular:

- for $k = 1$

$$\mathbf{N}^P = \mathcal{I}_6\,, \tag{16}$$

  so that the strain components are approximated by a constant function in each VE; in this case, $\hat{\boldsymbol{\varepsilon}}$ is a vector of 6 components;

- for $k = 2$

$$\mathbf{N}^P = \left[\begin{array}{ccc} \mathcal{I}_6 & \vdots & x_1\,\mathcal{I}_6 \end{array}\right. \left.\begin{array}{ccc} \vdots & x_2\,\mathcal{I}_6 \end{array}\right] \tag{17}$$

  so that the strain components are approximated by a linear function in each VE; in this case, $\hat{\boldsymbol{\varepsilon}}$ is a vector of 18 components.

- Second requirement for Π:

$$\int_{\Omega_E} (\boldsymbol{\varepsilon}^P)^T \Pi(\mathbf{u}^{\star\,h}) = \int_{\Omega_E} (\boldsymbol{\varepsilon}^P)^T \boldsymbol{\varepsilon}(\mathbf{u}^{\star\,h})\,dA \qquad \forall \boldsymbol{\varepsilon}^P \in P_{k-1}^{6\times 1}(\Omega_E)\,, \tag{18}$$

  i.e., taking into account equation (15),

$$\int_{\Omega_E} \hat{\boldsymbol{\varepsilon}}^T (\mathbf{N}^P)^T\, \Pi(\mathbf{u}^{\star\,h})\,dA = \int_{\Omega_E} \hat{\boldsymbol{\varepsilon}}^T (\mathbf{N}^P)^T\, \boldsymbol{\varepsilon}(\mathbf{u}^{\star\,h})\,dA \qquad \forall \hat{\boldsymbol{\varepsilon}} \in \mathbb{R}^{6\dim(P_{k-1})}\,, \tag{19}$$

5. Recalling (4) and integrating by parts, the r.h.s. of equation (19) becomes:

$$\int_{\Omega_E} \hat{\boldsymbol{\varepsilon}}^T (\mathbf{N}^P)^T\, \mathbf{L}\,\mathbf{u}^{\star\,h}\,dA = \hat{\boldsymbol{\varepsilon}}^T \left[\int_{\partial\Omega_E} (\mathbf{N}^P)^T\, \mathbf{N}_E\, \tilde{\mathbf{u}}^{\star\,h}\,dA - \int_{\Omega_E} (\mathbf{B}^P)^T\, \mathbf{u}^{\star\,h}\,dA\right] \tag{20}$$

where $\mathbf{N}_E$ is the matrix containing the components of the outward normal to the element boundary:

$$\mathbf{N}_E = \begin{bmatrix} n_1 & 0 & 0 \\ 0 & n_2 & 0 \\ 0 & 0 & 0 \\ n_2 & n_1 & 0 \\ 0 & 0 & n_2 \\ 0 & 0 & n_1 \end{bmatrix}. \tag{21}$$

Note that the operator $\mathbf{B}^P = \mathbf{L}^T\,\mathbf{N}^P$ indeed contains monomials of a basis of $P_{k-1}(\Omega_E)$.

Note that:

- for $k = 1$, the last term of equation (20) disappears;

- for $k = 2$, $\mathbf{B}^P$ is constant in Ω_E.

6. The integral at r.h.s. of equation (20) is written resorting to approximation (11) and split into a boundary and an interior contribution, respectively.

   This is done according to the properties of the approximation functions. In particular, boundary functions have unit value at corresponding nodes and zero at the other ones, plus they have zero area moments against any element of the canonical basis of $P_{k-1}(\Omega_e)$. Similarly each of the interior approximation functions is associated with a monomial of the canonical basis of $P_{k-1}(\Omega_e)$ and is such that the area-averaged moment against the corresponding monomial takes unit value, and zero value against the remaining ones. Furthermore, all the interior shape functions are identically zero at the polygon boundary nodes, hence null all over the boundary.

   This leads to:

$$\hat{\boldsymbol{\varepsilon}}^T \left[\int_{\partial\Omega_E} (\mathbf{N}^P)^T \, \mathbf{N}_E \, \mathbf{N}_\mathrm{b} \, \tilde{\mathbf{U}}^\star \, d\Gamma - \int_{\Omega_E} (\mathbf{B}^P)^T \, \mathbf{N}_\mathrm{i} \, \tilde{\mathbf{q}}^\star \, dA \right] = \hat{\boldsymbol{\varepsilon}}^T \left[\tilde{\mathbf{G}} \, \tilde{\mathbf{U}}^\star - \tilde{\mathbf{B}} \tilde{\mathbf{q}}^\star \right] ,$$

   where

$$\tilde{\mathbf{G}} = \int_{\partial\Omega_E} (\mathbf{N}^P)^T \, \mathbf{N}_E \, \mathbf{N}_\mathrm{b} \, d\Gamma \qquad \tilde{\mathbf{B}} = \int_{\Omega_E} (\mathbf{B}^P)^T \, \mathbf{N}_\mathrm{i} \, dA \, . \tag{22}$$

   It is now understood that the nature of the interior degrees of freedom $\tilde{\mathbf{q}}^\star$ is that of area-averaged moments of $\mathbf{u}^{\star\, h}$ against the monomials of the canonical basis of $P_{k-1}(\Omega_E)$.

   Introducing the matrix $\mathbf{G}$ and the vector $\mathbf{U}^\star$ as:

$$\mathbf{G} = \left[\tilde{\mathbf{G}} \, \vdots \, -\tilde{\mathbf{B}} \right] \qquad \mathbf{U}^\star = \left\{ \begin{array}{c} \tilde{\mathbf{U}}^\star \\ \mathbf{q}^\star \end{array} \right\} \tag{23}$$

   equation (22) becomes:

$$\hat{\boldsymbol{\varepsilon}}^T \int_{\Omega_E} (\mathbf{N}^P)^T \, \Pi(\mathbf{u}^{\star\, h}) \, dA = \hat{\boldsymbol{\varepsilon}}^T \, \mathbf{G} \, \mathbf{U}^\star \qquad \forall \hat{\boldsymbol{\varepsilon}} \, . \tag{24}$$

7. Representing the values of the projected strain with respect to the canonical basis of $P_k(\Omega_E)^{6\times 1}$, i.e. setting $\Pi(\mathbf{u}^{\star\, h}) = \mathbf{N}^P \boldsymbol{\Pi}^m \, \mathbf{U}^\star$, being $\boldsymbol{\Pi}^m$ the matrix operator associated with projection Π, equation (24) leads to:

$$\hat{\boldsymbol{\varepsilon}}^T \int_{\Omega_E} (\mathbf{N}^P)^T \, \mathbf{N}^P \, \boldsymbol{\Pi}^m \, \mathbf{U}^\star \, dA = \hat{\boldsymbol{\varepsilon}}^T \, \mathbf{G} \, \mathbf{U}^\star \qquad \forall \hat{\boldsymbol{\varepsilon}} \, . \tag{25}$$

   that gives:

$$\boldsymbol{\Pi}^m = \left[\int_{\Omega_E} (\mathbf{N}^P)^T \, \mathbf{N}^P \, dA \right]^{-1} \mathbf{G} \tag{26}$$

which is indeed explicitly computable.

8. Given the nonlinear character of the material laws of the fibre/matrix constituents of the unit cell, the equilibrium equation (13) needs be linearized with respect to the displacement field and solved via Newton iterations. Integration of the evolutive equations governing the material response is performed adopting a time step procedure, so that quantities at the previous time step t_n are denoted with the subscript $_n$ while at actual time t have no subscripts. Moreover, for the average strain $\mathbf{E}$ at the typical load step, the iterative counter is indicated by (r). In what follows, the terms arising from the consistent linearization of equation (13) are reported, omitting the dependence of the incremental solution on the index (r) for compactness. The linearization at time step t is composed of two distinct contributions: the *consistent* one, plus another one serving as a *stabilization* term supplied in order to cure the rank deficiency induced by the definition of the projector operator $\mathbf{\Pi}$ [6]. One obtains:

$$\begin{aligned} 0 &= \int_{\Omega_E} [\mathbf{\Pi}(\delta \mathbf{u}^{\star h}_{(r)})]^T \, \mathbf{C}_{(r)} \, [\mathbf{\Pi}(\Delta \mathbf{u}^{\star h}_{(r)}) + \mathbf{E}] \, dA \\ &+ [\delta \mathbf{u}^{\star h}_{(r)} - \mathbf{\Pi}^s(\delta \mathbf{u}^{\star h}_{(r)})]^T \, \tau^s_n \, [\Delta \mathbf{u}^{\star h}_{(r)} - \mathbf{\Pi}^s(\Delta \mathbf{u}^{\star h}_{(r)})] \, . \end{aligned} \tag{27}$$

In the above form, the integral term stems from the consistent linearization, with $\mathbf{C}_{(r)}$ the material tangent stiffness operator. The second term is indeed the stabilizing one, where τ^s_n and $\mathbf{\Pi}^s$ are a suitable parameter and a projection operator, respectively.

Once the projection operator $\mathbf{\Pi}^m$ is evaluated, equation (27) takes the form:

$$\begin{aligned} 0 &= \int_{\Omega_E} [\mathbf{N}^P \mathbf{\Pi}^m \, \delta \mathbf{U}^{\star}_{(r)}]^T \, \mathbf{C}_{(r)} \, [\mathbf{N}^P \mathbf{\Pi}^m \, \Delta \mathbf{U}^{\star}_{(r)} + \mathbf{E}] \, dA \\ &+ [(\mathbf{I} - \mathbf{\Pi}^s) \, \delta \mathbf{U}^{\star}_{(r)}]^T \, \tau^s_n \, [(\mathbf{I} - \mathbf{\Pi}^s) \, \Delta \mathbf{U}^{\star}_{(r)}] \, . \end{aligned} \tag{28}$$

Hence, the incremental equilibrium equation (13) takes the form:

$$\mathbf{0} = \left(\mathbf{K}_{c,(r)} + \mathbf{K}_s \right) \Delta \mathbf{U}^{\star}_{(r)} + \mathbf{B} \, , \tag{29}$$

where

$$\mathbf{K}_{c,(r)} = (\mathbf{\Pi}^m)^T \int_{\Omega_E} (\mathbf{N}^P)^T \mathbf{C}_{(r)} \, \mathbf{N}^P dA \, \mathbf{\Pi}^m \tag{30}$$

$$\mathbf{K}_s = \tau^s_n \, (\mathbf{I} - \mathbf{\Pi}^s) \tag{31}$$

$$\mathbf{B} = (\mathbf{\Pi}^m)^T \int_{\Omega_E} (\mathbf{N}^P)^T dA \, \mathbf{E} \tag{32}$$

are the consistent stiffness matrix, the stabilizing stiffness matrix, and the nodal force vector, respectively. The form of $\mathbf{K}_s$, needed to preserve the coercivity of the system.

9. According to standard VEM technology [6], the easiest form for $\mathbf{\Pi}^s$ is provided by a standard projector from the space of virtual element displacements degrees of freedom $\mathbf{U}^\star$ to the corresponding polynomial counterpart of degree k, i.e. $P_k^{3\times 1}(\Omega_E)$, defined as the unique matrix-valued function satisfying the following relation:

$$< \mathbf{\Pi}^s \mathbf{U}^\star, \mathbf{v} > = < \mathbf{U}^\star, \mathbf{v} > , \quad \forall \mathbf{v} \in P_k^{3\times 1}(\Omega_E) \tag{33}$$

where $< \cdot, \cdot >$ indicates the standard Euclidean scalar product. Explicit computation of the above scalar product and hence of the stabilizing projector $\mathbf{\Pi}^s$ requires representation of the $\mathbf{q}$ vector quantities with respect to the approximation functions of the space of virtual displacements. This is always possible since such a space contains $P_k^{3\times 1}(\Omega_E)$ [7]. Denoting $\mathbf{D}$ as the corresponding change of basis operator, which can be found in [2, 3], by substitution into (33), it follows:

$$\mathbf{\Pi}^s = \mathbf{D}\left(\mathbf{D}^{\mathrm{T}}\mathbf{D}\right)^{-1}\mathbf{D}^{\mathrm{T}} . \tag{34}$$

The choice for the stabilizing parameter τ_n^s is adopted according to what is proposed in [2], namely a third of the trace of the material tangent stiffness evaluated at the centroid of the element at the previous load step; in this way the stabilizing parameter is not influential in the linearization of the equilibrium equation at time step t greatly simplifying the numerical solution.

4 Numerical results

The present section is devoted to validation and accuracy assessment of the proposed VEM technology in the nonlinear analysis of elasto-plastic and visco-plastic composites with respect to established methods, and, more specifically, to proving the VEM method efficiency as a computational cost-effective tool for fast and reliable analysis. The idea is to investigate modern advanced composite materials with fibre reinforcement characterized by complex material constitutive behavior as for instance with elastic fibres and plastic or viscoplastic matrix behavior. In the context of multiscale analysis, when dealing with components made of this type materials, an efficient and accurate numerical tool for solving the microscopic level of the problem may be key in terms of computational efficiency. Is is noted, moreover, that from a technical point of view, a numerical approach in the aforementioned context is mandatory in the majority of cases, since analytical or semi-analytical methods [5, 4] are unpractical for the more complex material setups, as for instance randomly distributed fibres, complex fibre shapes, generally not not solvable by such approaches [10].

In the following, reference is made to composite arrangements characterized by square unit cell and different nonlinear material behavior; the main goal being to apply the previously introduced methodology to compute mechanical response under the application of a macroscopic strain through some specified loading history, for the cases in which material nonlinearity is encountered.

4.1 Accuracy - elastic composites

??? Validation still needs a fair assessment of the exact solution for the overall properties. ???

	Tri	Poly	Quad
Mesh 1	–	144	201
Mesh 2	–	576	689
Mesh 3	–	2304	2529
Mesh 4	–	9216	9665
Overkilling	149249	–	–

Table 1: Meshing discretizations in terms of number of vertices for examined case $v_f = 0.4$.

4.2 Accuracy - Elasto-plastic composites

This section aims at assessing accuracy of the proposed method for $k = 1$ and $k = 2$ by comparison with standard Lagrange finite element solutions, when, as in the previous case, a uniform QUAD/POLY unit cell mesh is adopted (see Fig. 2). A composite with elastic fibres and elasto-plastic matrix is considered, such that material parameters for

the fibre and for the matrix are $E^f = 410$ GPa, $\nu^f = 0.19$, $E^m = 75$ GPa, $\nu^m = 0.33$, respectively. The matrix material obeys a classical isotropic Von Mises plastic constitutive law with yield stress $\sigma_y = 2.37$ GPa; no strain hardening is considered. The volume fraction taken into consideration is $v_f = 0.2$. Monotonic proportional loading histories for the single overall strain components (cf. Eq. (10)) are considered stemming from zero to a specified value of 0.1; correspondingly, the homologue effective stress components are plotted in Fig. 5, respectively, for linear and quadratic elements, reporting VEM solutions and Lagrangian finite element ones as a reference, with Mesh 3 as per Table 1, i.e. with a uniform discretization of the fibre/matrix domain. For the sake of compactness the acronyms $Q4$ and $Q9$ are here adopted, respectively, for quadrilateral 4−node and 9−node isoparametric displacement-based Lagrangian finite elements. The computed solutions seem in optimal agreement and thus validate the proposed VEM methodology for both QUAD/POLY discretizations of the unit cell domain, confirming the robustness and appeal of the numerical tool in computing the overall response of the composite material.

4.3 Accuracy - Visco-plastic composites

This section is designed to prove one of the main feature of the VEM technology as an efficient asset in reducing computational cost, hence computational time, when a typical multiscale structural analysis if performed. The feature under consideration is the generalized concept of polygonal mesh *simplicity* as opposed to standard *conformity* in finite element discretization, which, in general, permits to discretize and refine VEM polygonal meshes with broader versatility with respect to FEM meshes saving on vertices along the reticulation. In the present application, based on the fact that for a composite with sufficiently high an η ratio, the displacement field varies slowly among the fibre subdomain, the possibility of coarsening just locally its discretization, still retaining sufficiently low fineness of mesh size over the rest of the domain, comes in handy. This is exactly the idea exploited in this numerical test, which is designed in the following manner: numerical results pertaining to uniform polygonal Mesh 3 (see Table 1) are confronted with an ad hoc designed mesh which comprises a single polygon inside the fibre (so called core region for the fibre), two refined circular crown shaped regions across fibre/matrix interface (these are mandatory as displacement gradient components may be high across the aforementioned interface, requiring high resolution), and a matrix region with reasonably fine size. A pictorial view of such a mesh is given in Fig. 3 and, in the following, will be denoted as *crown*. The overall ratio between uniform and crown mesh number of degrees of freedom is circa 4. The aim is to prove that, despite its smart coarseness, results pertaining to crown mesh are equally accurate than those obtained with its uniform (finer) counterpart.

Performed simulations refer to both elasto-plastic and visco-plastic composites. In particular, in the former case, material parameters adopted in the previous test are

adopted doubling the fibre Young modulus; in the latter, material parameters as of constitutive model presented in section 2 are $E^f = 410$ GPa, $\nu^f = 0.19$, $E^m = 7.5$ GPa, $\nu^m = 0.33$, $\sigma_y = 0.2$ GPa. (Gli altri parametri vanno linkati ai simboli del paper che non corrispondono a quelli del legame costitutivo). Simulations refer to simple monotonic loading histories and results are performed for $k = 1$ and $k = 2$ order of accuracy. As can be inspected in Figs. 6, 7, respectively, the relative errors in terms of effective response are practically less than 5% at maximum, a relative threshold which is indeed acceptable in the light of the previous introductory remarks. It is of interest observing that the computational times for *crown* mesh are roughly 8 times smaller than those needed for the uniform mesh discretization. This impressive results indeed proves the stated point and indicates the efficiency of the proposed methodology in exploiting the relaxed mesh conformity requirements dealing with complex domain shapes.

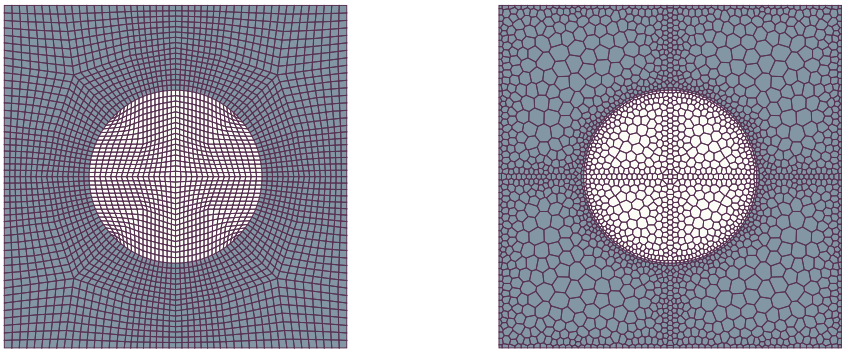

(a) (b)

Figure 2: *Uniform* unit cell meshes for examined case $v_f = 0.2$; (a) quadrilaterals (QUAD); (b) polygons (POLY).

5 Conclusion

- A virtual element method of higher order has been presented for the homogenization of fibre-reinforced composite materials with doubly periodic square lattices and circular fibre inclusions;
- The methodology has been tested and validated on a number of unit cell setups for quadrilateral and Voronoi tessellations mesh types;
- The strength of the proposed approach relies in the ability to accurately deal with complex geometries, flexibility in local mesh refinement, and polynomial degree elevation;

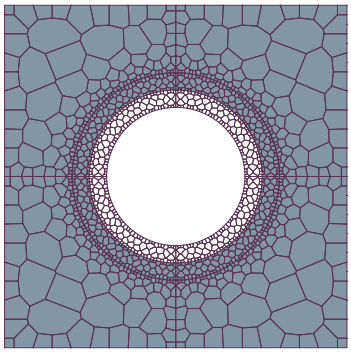

Figure 3: *Crown* unit cell mesh for examined case $v_f = 0.2$. Local mesh refinement across fibre/matrix interface with two circular crown regions with very fine POLY-mesh and a single polygon with 140 edges for the fibre core.

- Future investigations of this study include treatment of complex material constitutive behavior, general representative unit cells and the case of complex inclusion shapes.

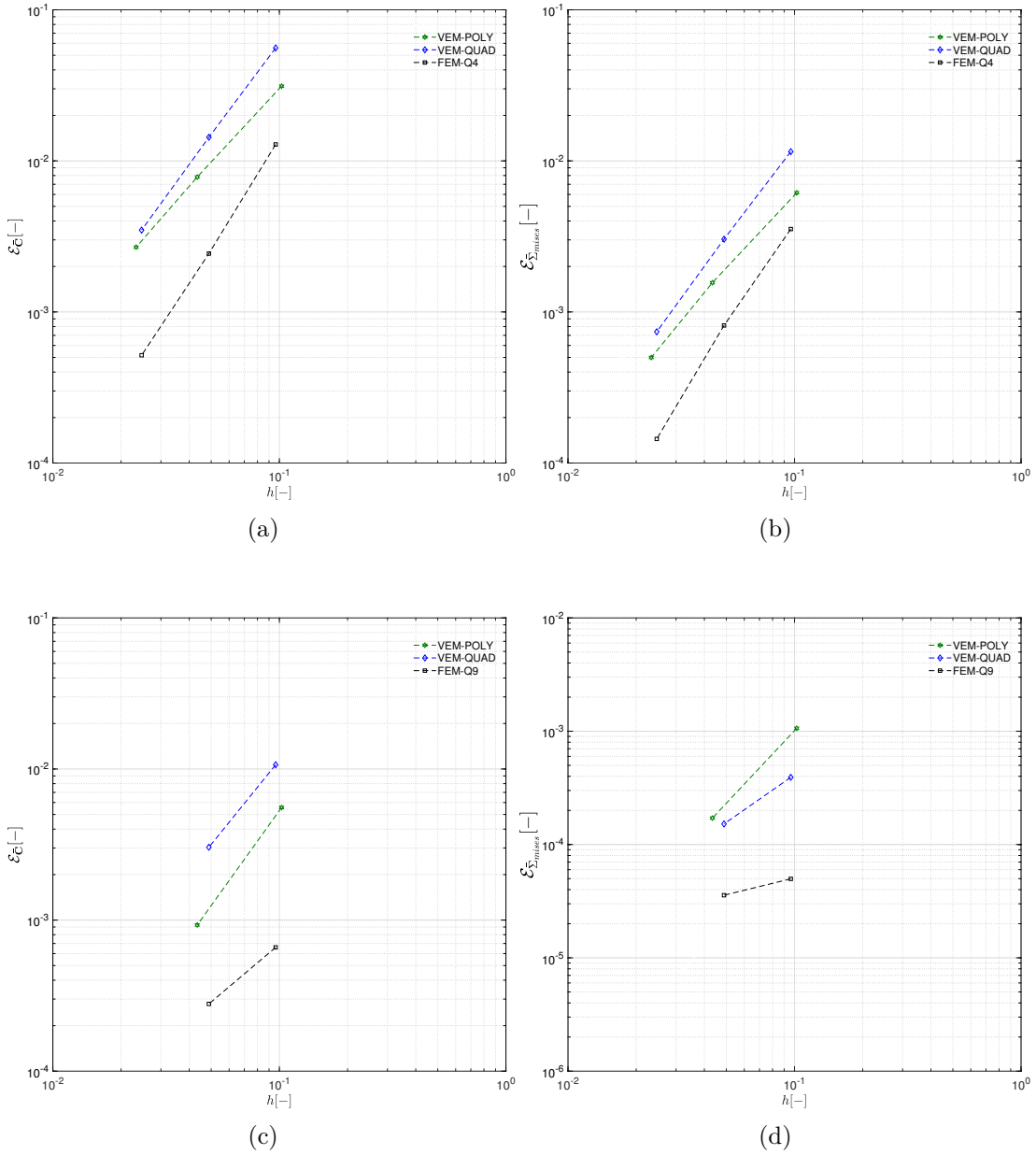

(a) (b)

(c) (d)

Figure 4: Accuracy assessment for various error measures. Square unit cell, $v_f = 0.4$. Compared methods: VEM with triangles, polygons, quadrilaterals; reference overkilling solution computed with FEM quadratic quadrilaterals.

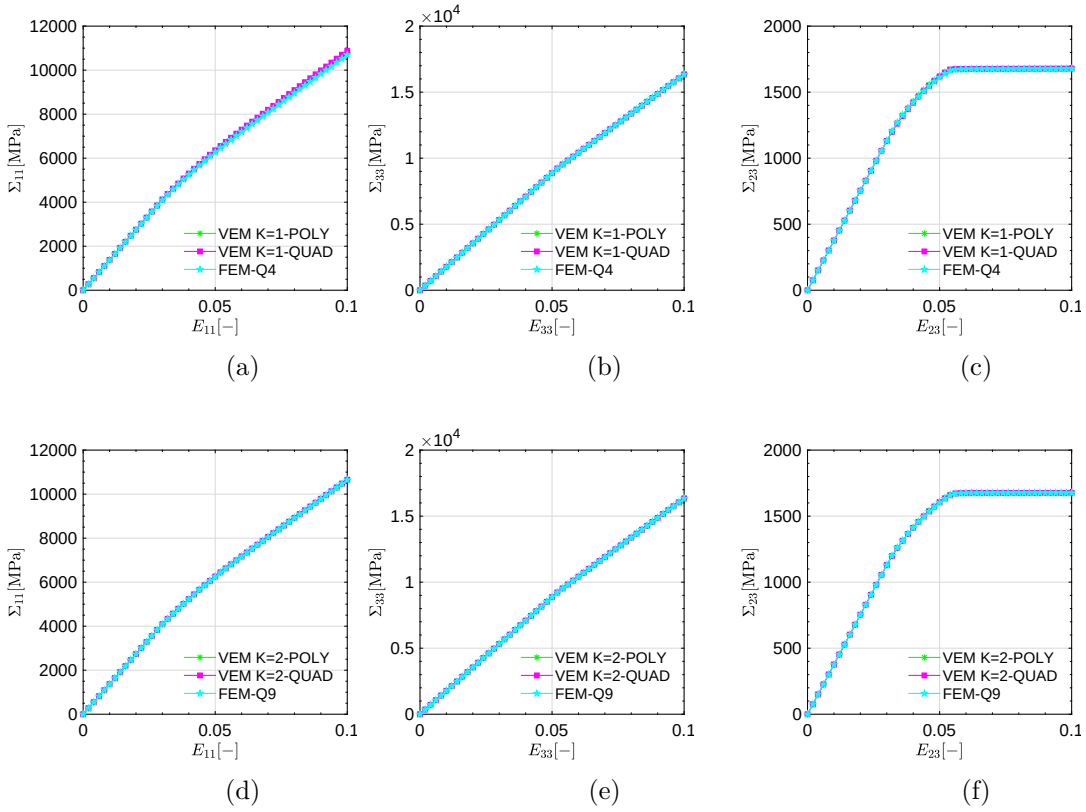

Figure 5: Elastoplastic fibre reinforced composite. $v_f = 0.2$. $k = 1$ (a-b-c), $k = 1$ (d-e-f).

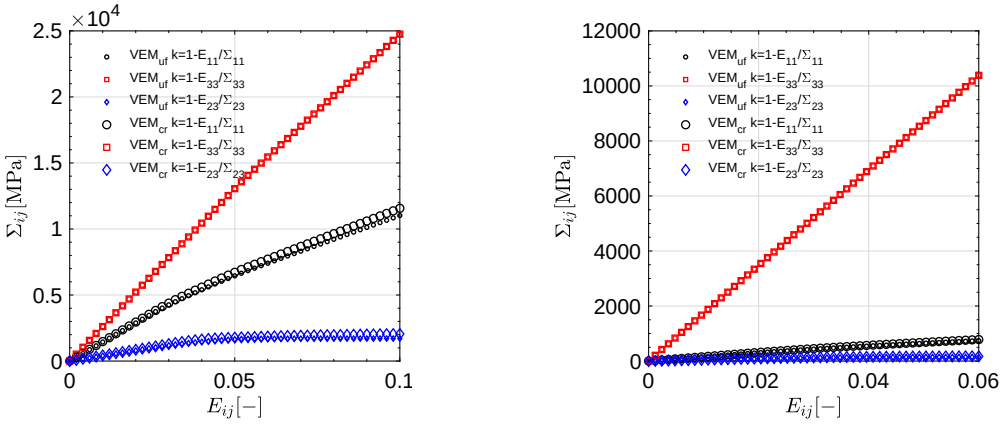

(a) (b)

Figure 6: Efficiency of *crown* vs. *uniform* polygonal mesh for elastoplastic (a) and viscoplastic (b) composite. $k = 1$, $v_f = 0.2$.

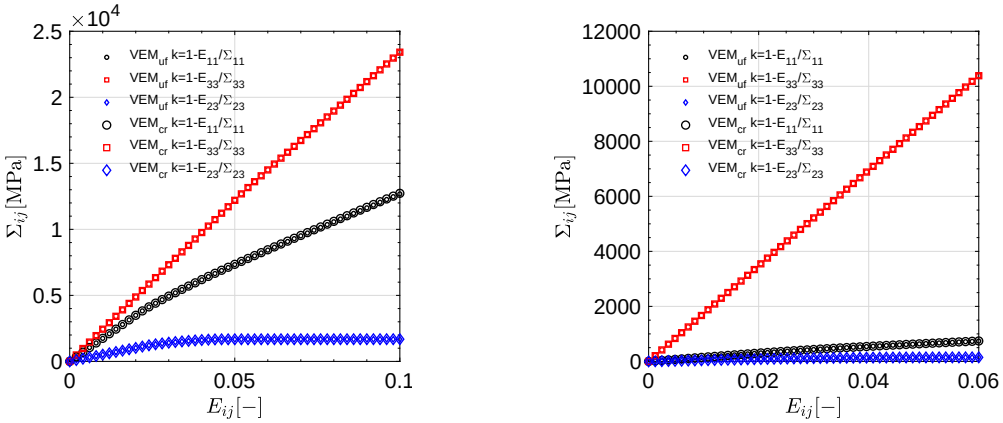

(a) (b)

Figure 7: Efficiency of *crown* vs. *uniform* polygonal mesh for elastoplastic (a) and viscoplastic (b) composite. $k = 2$, $v_f = 0.2$.

References

[1] B. Ahmad, A. Alsaedi, F. Brezzi, L. D. Marini, and A. Russo, *Equivalent projectors for virtual element methods*, Comput. Math. Appl. **66** (2013), no. 3, 376–391.

[2] E. Artioli, L. Beirão da Veiga, C. Lovadina, and E. Sacco, *Arbitrary order 2D virtual elements for polygonal meshes: Part I, elastic problem*, Computational Mechanics **60** (2017), 355–377.

[3] E. Artioli, L. Beirão da Veiga, C. Lovadina, and E. Sacco, *Arbitrary order 2D virtual elements for polygonal meshes: Part II, inelastic problem*, Computational Mechanics **60** (2017), 643–657.

[4] E. Artioli and P. Bisegna, *Effective longitudinal shear moduli of periodic fibre-reinforced composites with functionally-graded fibre coatingss*, Int. J. Solids Struct. **50** (2013), 1154–1163.

[5] E. Artioli, P. Bisegna, and F. Maceri, *Effective longitudinal shear moduli of periodic fibre-reinforced composites with radially-graded fibres*, Int. J. Solids Struct. **47** (2010), 383–397.

[6] L. Beirão da Veiga, F. Brezzi, A. Cangiani, G. Manzini, L. D. Marini, and A. Russo, *Basic principles of virtual element methods*, Math. Models Methods Appl. Sci. **23** (2013), no. 1, 199–214.

[7] L. Beirão da Veiga, F. Brezzi, and L. D. Marini, *Virtual elements for linear elasticity problems*, SIAM J. Numer. Anal. **51** (2013), no. 2, 794–812.

[8] V. Carvelli and A. Taliercio, *Micromechanical model for the analysis of unidirectional elasto-plastic composites subjected to 3D stresses.*, Mechanical Research Communications **26** (1999), 547 – 553.

[9] C. Czarnota, K. Kowalczyk-Gajewska, A. Salahouelhadj, M. Martiny, and S. Mercier, *Modeling of the cyclic behavior of elastic-viscoplastic composites by the additive tangent Mori-Tanaka approach and validation by finite element calculations*, International Journal of Solids and Structures **56-57** (2015), 96 – 117.

[10] D. Joyce, W.J. Parnell, R.C. Assier, and I.D. Abrahams, *An integral equation method for the homogenization of unidirectional fibre-reinforced media; antiplane elasticity and other potential problems*, accepted, and online on: http://rspa.royalsocietypublishing.org/ (2017).

[11] C. Mareau and S. Berbenni, *An affine formulation for the self-consistent modeling of elasto-viscoplastic heterogeneous materials based on the translated field method*, International Journal of Plasticity **64** (2015), 134 – 150.

[12] S. Marfia, *Micro-macro analysis of shape memory alloy composites*, Int. J. of Solids Struct. **42** (2005), 3677–3699.

[13] S. Marfia and E. Sacco, *Micromechanics and homogenization of sma-wire-reinforced materials*, Journal of Applied Mechanics **72** (2005), 259–268.

[14] T. Mura, *Micromechanics of defects in solid*, Martinus, 1987.